



HAL
open science

A two-phase model for sheet flow regime based on dense granular flow rheology

Thibaud Revil-Baudard, Julien Chauchat

► **To cite this version:**

Thibaud Revil-Baudard, Julien Chauchat. A two-phase model for sheet flow regime based on dense granular flow rheology. *Journal of Geophysical Research*, 2013, pp.10.1029/2012JC008306. 10.1029/2012JC008306 . hal-00860868

HAL Id: hal-00860868

<https://hal.science/hal-00860868>

Submitted on 11 Sep 2013

HAL is a multi-disciplinary open access archive for the deposit and dissemination of scientific research documents, whether they are published or not. The documents may come from teaching and research institutions in France or abroad, or from public or private research centers.

L'archive ouverte pluridisciplinaire **HAL**, est destinée au dépôt et à la diffusion de documents scientifiques de niveau recherche, publiés ou non, émanant des établissements d'enseignement et de recherche français ou étrangers, des laboratoires publics ou privés.

1 A two-phase model for sheet flow regime based on
2 dense granular flow rheology

T. Revil-Baudard¹ and J. Chauchat¹

¹Laboratoire des Ecoulements

Géophysiques et Industriels, UMR 5519,

UJF, INPG, Grenoble, France

3 **Abstract.** A two-phase model having a $\mu(I)$ rheology for the intergran-
4 ular stresses and a mixing length approach for the turbulent stresses is pro-
5 posed to describe the sheet flow regime of sediment transport. In the model
6 two layers are considered, a dilute suspension layer and a dense sediment bed
7 layer. The concentration profile is obtained from the dilatancy law $\phi(I)$ in
8 the sediment bed layer and from a Rouse profile in the suspension layer. The
9 comparison of velocity profile, concentration profile and macroscopic param-
10 eters (sediment flux, thickness and roughness) with experimental data shows
11 a good agreement. These comparisons demonstrate that the dense granular
12 rheology is relevant to describe intense bed-load transport in turbulent regime
13 (sheet flow). The transition from the dense static bed to the dilute suspen-
14 sion is well described by the present model. Also, the different regimes of the
15 dense granular rheology seems to be able to capture the transition between
16 collision dominant and turbulent fluctuations dominant sheet flows, depend-
17 ing on the particles characteristic.

1. Introduction

18 The sheet flow regime of sediment transport is associated to extreme events such as
19 sand storms, river floods or storm waves in the surf zone. Because of the huge amount
20 of sediment transported in this regime it is especially important for the understanding
21 of the morphological evolution and the stability of constructions in riverine and coastal
22 environments.

23 From a physical point of view the sheet flow regime is characterized by a high bed shear
24 stress (*e.g.* *Hanes and Bowen* [1985]) represented by the so-called Shields number θ , ratio
25 of the force exerted by the fluid on the sediment bed over the apparent weight of a single
26 particle. It is usually considered that sheet flow occurs for Shields number higher than
27 0.5 which corresponds to roughly ten times the critical Shields number θ_c in the turbulent
28 regime. The flow is strong enough to wash out bedforms, the sediment bed becomes flat,
29 and the thickness of the bed-load layer δ_s is of order of ten times the particle's size d_p .
30 It is widely accepted that particle-particle interactions, such as collisions and frictional
31 interactions, and fluid turbulent velocity fluctuations are the key mechanisms controlling
32 the sheet flow (*Bagnold* [1956]; *Jenkins and Hanes* [1998] amongst others).

33 In this paper, we focus on uniform steady sheet flows. Such sheet flow conditions
34 have been studied in small scale experiments by *Wilson* [1966, 1989]; *Nnadi and Wilson*
35 [1992]; *Sumer et al.* [1996]; *Gao* [2008] and *Cowen et al.* [2010]. In these studies, velocity
36 and concentration measurements as well as image analyses were performed for different
37 sediment types and different flow conditions.

38 First attempts in modeling sheet flow have been proposed by *Hanes and Bowen* [1985]
39 or *Wilson* [1987], amongst others. In these models the concentration profile is prescribed
40 and the intergranular stresses are given by a phenomenological law (*e.g.* *Bagnold* [1954]).
41 Over the past fifteen years, two-phase models, based on kinetic theory of granular flows
42 to describe intergranular stresses, has been applied with some success to model the sheet
43 flow regime *e.g.* *Jenkins and Hanes* [1998]; *Greimann and Holly* [2001]; *Hsu et al.* [2004];
44 *Longo* [2005]; *Amoudry et al.* [2008]. In these models, the kinetic theory has been stated
45 for situations in which collisional interactions are the dominant mechanism of momentum
46 transfer. The concentration profile is obtained from a balance between collisional interac-
47 tions and gravity as a result of the model. The collisional shear stresses are linked to the
48 strength of the particles velocity fluctuations represented by the granular temperature.
49 For this new variable an equation for energy conservation has to be solved with complex
50 boundary conditions in addition to the momentum conservation equation for the partic-
51 ulate phase. *Berzi* [2011] has proposed a simplified analytical solution for the collisional
52 sheet flow regime based on a layer decomposition: a collisional layer based on the kinetic
53 theory of granular flows and a macro-viscous layer describing the transition from the col-
54 lisional regime to the quasi-static one (*i.e.* fixed bed). These last layer is introduced to
55 circumvent one of the main limitation of the kinetic theory of granular flows, the modeling
56 of repeated collisions and/or enduring contacts [*Jenkins*, 2006].

57 Recent improvements in the understanding of the liquid regime of dense granular
58 flows [*GDR midi*, 2004; *Cassar et al.*, 2005; *Forterre and Pouliquen*, 2008; *Boyer et al.*,
59 2011] has led to the proposition of a visco-plastic rheology. This rheology exhibits a thresh-
60 old of motion, controlled by the static friction coefficient and the particulate pressure, and

61 a shear rate dependence of the particulate shear stress characteristic of a viscous-like be-
 62 havior. It has been used with some success by *Ouriemi et al.* [2009] and *Aussillous et al.*
 63 [2012] to model bed-load transport in laminar shearing flows. The author's two-phase
 64 model is based on the phenomenological granular rheology $\mu(I)$ for the intergranular
 65 stresses [*Forterre and Pouliquen*, 2008]. The concentration profile is either assumed con-
 66 stant in the moving sediment layer or obtained from the $\phi(I)$ phenomenological law [*Boyer*
 67 *et al.*, 2011].

68 The phenomenological laws $\mu(I)/\phi(I)$ are based on dimensional analysis where I rep-
 69 resents the dimensionless number controlling the friction coefficient μ and the volume
 70 fraction ϕ [*Forterre and Pouliquen*, 2008]. It can be interpreted as the ratio of a vertical
 71 time scale of rearrangement to an horizontal time scale of deformation. When the deforma-
 72 tion time scale is large (small shear rate) compared with the time scale of rearrangement
 73 the granular media is in the quasi-static regime ($I \ll 1$). When the parameter I is of
 74 order unity ($I \approx 1$), the granular media is in the liquid regime of dense granular flows.
 75 In this regime, the concentration ϕ decreases and the friction coefficient μ increases with
 76 the dimensionless number I . When the parameter I is much greater than unity ($I \gg 1$),
 77 the granular media is in the gaseous regime.

78 Following *Courrech du Pont et al.* [2003] and *Cassar et al.* [2005] three regimes can
 79 be observed for the vertical time scale of rearrangement: free fall, viscous or turbulent,
 80 leading to the three corresponding regimes for the phenomenological rheology. The dry
 81 granular case pertains to the free fall regime and has been extensively studied over the
 82 last two decades *e.g.* *Forterre and Pouliquen* [2008] and references therein. In the viscous
 83 regime, *Boyer et al.* [2011] have proposed relationships for the two constitutive laws $\mu(I)$

84 and $\phi(I)$ based on annular shear cell experiments. These relationships are valid in the
85 range $\phi \in [0.3 ; 0.585]$ for spheres.

86 In this paper a two phase model for turbulent flows inspired from the early work of
87 *Ouriemi et al.* [2009] and *Aussillous et al.* [2012] in the laminar case is presented. In
88 the turbulent case the concentration decreases continuously from the static bed up to
89 the suspension [*Nnadi and Wilson*, 1992; *Sumer et al.*, 1996]. The phenomenological
90 laws $\mu(I)/\phi(I)$ are used to account for the intergranular stresses and the dilatancy effects
91 inside the sediment bed layer. In the suspension a Rouse profile is assumed to represent
92 the suspended sediment transport. As a first step a simple mixing-length model is used
93 to model the fluid Reynolds stresses. The main objective of the present contribution is
94 to propose an alternative approach to the kinetic theory of granular flows to describe
95 the intergranular stresses based on the dense granular flow rheology for the modeling
96 of sheet flow regime. The velocity and concentration profiles predicted by the present
97 model are compared to existing experimental data from the literature. The evolution
98 of the sediment transport rate, the moving sediment layer thickness and the equivalent
99 roughness are compared to empirical correlations and available experimental data for a
100 wide range of Shields number. Modeling of transitions from the dense static bed to the
101 dilute suspension and between collisional dominant and turbulent fluctuations dominant
102 sheet flows are also investigated in the present work.

103 The model formulation and numerical algorithm are presented in section 2. The results
104 are presented in section 3 while section 4 is dedicated to the discussion.

2. Model formulation

105 A sketch of the flow is presented in figure 1. The domain is decomposed into two layers:
 106 a Fluid Layer (FL) and a Sediment Bed Layer (SBL).

107 In the FL, the turbulent fluid flow is driven by gravity and exerts a shear stress on the
 108 SBL. In the SBL, the fluid-particles mixture is set in motion by this fluid shear stress and
 109 the gravity. We only consider situations where this fluid shear stress is high enough to
 110 set a thick layer of sediment particles in motion (*i.e.* $\theta \gg \theta_c$ and $\delta_s \gg d_p$). The two
 111 layers, FL and SBL, are solved separately in the model. In the FL only the fluid phase
 112 momentum equation is solved. In the SBL a two-phase model is used with momentum
 113 equations for both fluid and particulate phases.

2.1. Two-phase model in the SBL layer

114 The present model is based on *Jackson* [2000]'s two-phase equations (1)-(4)

$$\frac{D\rho_f\epsilon\vec{u}^f}{Dt} = -\vec{\nabla}P^f\bar{I} + \vec{\nabla}.\bar{\tau}^f + \vec{\nabla}.\bar{R}^f + \epsilon\rho_f\vec{g} + n\vec{f}, \quad (1)$$

$$\frac{D\rho_p\phi\vec{u}^p}{Dt} = -\vec{\nabla}P^p\bar{I} + \vec{\nabla}.\bar{\tau}^p + \phi\rho_p\vec{g} - n\vec{f}, \quad (2)$$

$$\frac{D\rho_f\epsilon}{Dt} = \frac{\partial\epsilon}{\partial t} + \vec{\nabla}.\left(\epsilon\vec{u}^f\right) = 0, \quad (3)$$

$$\frac{D\rho_p\phi}{Dt} = \frac{\partial\phi}{\partial t} + \vec{\nabla}.\left(\phi\vec{u}^p\right) = 0, \quad (4)$$

115 in which ϵ and ϕ represent fluid and particles volume fractions. The other variables are
 116 defined, for a generic phase k , as follows: ρ_k represents the true density, \vec{u}^k corresponds

117 to the volume averaged velocity, P^k is the pressure, $\overline{\tau^k}$ represents the shear stress, where
 118 k stands either for the fluid phase f or the particulate phase p . $\overline{R^f}$ corresponds to the
 119 fluid Reynolds stresses. The term $n \overrightarrow{f}$ represents the interactions between the fluid and
 120 the particulate phase and \overrightarrow{g} classically corresponds to the gravitational acceleration.

121 In this paper we focus on a unidirectional and steady sheet flow therefore the two-
 122 phase equations (1-4) simplifies with all dependencies in t , x and y vanishing. As we
 123 are interested in the steady state solution, we further assumes that the vertical velocities
 124 of both phases vanish. Therefore, the mass conservation equation (3)-(4) are trivially
 125 satisfied. The variables that appears in the resulting equations are τ_{xz}^f , R_{xz}^f , ϵ , ϕ , P^f , P^p ,
 126 $n f_x$, and $n f_z$ that only depend on the vertical upward direction z . The simplified system
 127 of equations reads:

$$0 = \frac{d\tau_{xz}^f}{dz} + \frac{dR_{xz}^f}{dz} - n f_x + \epsilon \rho_f g \sin \beta \quad (5)$$

$$0 = \frac{d\tau_{xz}^p}{dz} + n f_x + \phi \rho_p g \sin \beta \quad (6)$$

$$0 = -\frac{dP^f}{dz} - n f_z - \epsilon \rho_f g \cos \beta \quad (7)$$

$$0 = -\frac{dP^p}{dz} + n f_z - \phi \rho_p g \cos \beta \quad (8)$$

$$\epsilon + \phi = 1 \quad (9)$$

128 The system (5)-(9) is similar to the one proposed by *Ouriemi et al.* [2009] for the laminar
 129 case except by the presence of the term R_{xz}^f for the fluid Reynolds stresses.

130 Phases interactions

131 Following *Jackson* [2000], the terms nf_x and nf_z represent all the forces acting at the
 132 fluid particles interface such as buoyancy, drag, lift, Basset forces. In sediment transport
 133 problems the dominant interaction forces are the buoyancy and the drag forces [*Hsu et al.*,
 134 2003, 2004; *Bombardelli and Jha*, 2009]. In the vertical direction the buoyancy force is
 135 the only interaction force at steady state:

$$nf_z = -\phi \frac{dP^f}{dz}.$$

136 In the horizontal direction, the fluid-particle interactions are the generalized buoyancy
 137 force, due to the fluid stresses acting on the fluid-particle interfaces, and the drag force
 138 induced by the velocity difference between the fluid and the particles

$$nf_x = \phi \frac{d\tau_{xz}^f}{dz} + C_D (U - u^p) \quad (10)$$

139 In the second term of this relationship C_D represents the drag coefficient. Following
 140 *Jenkins and Hanes* [1998] and *Hsu et al.* [2004], the Dallavalle formulae is used with
 141 *Richardson and Zaki* [1954]'s correction:

$$C_D = \frac{\rho_f \phi}{d_p (1 - \phi)^{3.1}} \left(0.3 (U - u^p) + 18.3 \frac{\eta_f}{\rho_f d_p} \right), \quad (11)$$

142 where $U = (1 - \phi) u^f + \phi u^p$ represents the volume averaged mixture velocity.

143 Introducing the buoyancy force in the vertical momentum equations (7)-(8) an hydro-
 144 static pressure distribution is obtained for both phases. This is consistent with *Berzi*
 145 [2011]'s analytical solution.

$$\frac{dP^f}{dz} = \rho_f g \cos \beta \quad \text{and} \quad \frac{dP^p}{dz} = \phi(\rho_p - \rho_f)g \cos \beta. \quad (12)$$

146 Introducing the expression of $n f_x$ (10) in the horizontal momentum equations (5)-(6)
 147 leads to the following system of equations:

$$0 = \frac{dR_{xz}^f}{dz} + \epsilon \frac{d\tau_{xz}^f}{dz} - C_D (U - u^p) + \epsilon \rho_f g \sin \beta \quad (13)$$

$$0 = \frac{d\tau_{xz}^p}{dz} + \phi \frac{d\tau_{xz}^f}{dz} + C_D (U - u^p) + \phi \rho_p g \sin \beta \quad (14)$$

148 Closures of the fluid stresses

149 Following the proposition of *Ouriemi et al.* [2009] a Newtonian form of the fluid phase
 150 viscous stresses is assumed

$$\tau_{xz}^f = \eta_e \frac{dU}{dz} \quad (15)$$

151 where η_e is the effective viscosity. As no theoretical model exists for dense suspension,
 152 *Ouriemi et al.* [2009] proposed to use the Einstein's viscosity $\eta_e/\eta_f = (1 + 5\phi/2)$. This
 153 choice was not definitely settled in this paper. Recently *Boyer et al.* [2011] have measured
 154 the rheology of an isodense granular suspension in a pressure controlled annular shear cell
 155 experiment. The authors have proposed the following relationship:

$$\frac{\eta_e}{\eta_f} = 1 + \frac{5}{2}\phi \left(1 - \frac{\phi}{\phi^m}\right)^{-1}, \quad (16)$$

156 which allows to recover Einstein's viscosity at low concentration and diverges at the
 157 maximum packing fraction ϕ^m with a behavior similar to Krieger-Dougherty's formulation
 158 [*Krieger and Dougherty*, 1959].

159 The fluid Reynolds stresses R_{xz}^f are closed using an eddy viscosity concept based on a
 160 mixing length approach:

$$R_{xz}^f = \eta_t \frac{dU}{dz} \quad \text{with} \quad \eta_t = \rho_f (1 - \phi) l_m^2 \left| \frac{dU}{dz} \right|. \quad (17)$$

161 The mixing length l_m is parameterized following *Li and Sawamoto* [1995] by

$$l_m = \kappa \int_0^z \frac{\phi^m - \phi}{\phi^m} dz, \quad (18)$$

162 where κ is the Von Karman constant. This mixing length formulation has been used with
 163 some success by *Dong and Zhang* [1999] in a two-phase model for oscillatory sheet flow. In
 164 this formulation the mixing length is weighted by the integral of the concentration profile.
 165 Considering the limit case of a static bed at maximum volume fraction, the turbulence is
 166 fully damped in the bed and the classical linear Prandtl mixing length $l_m = \kappa (h_p - z)$ is
 167 recovered in a clear fluid boundary layer.

168 The choice of a mixing length model is justified by the uniformity and the steadiness of
 169 the flow. Moreover, such a modeling for the fluid Reynolds stresses is coherent with the
 170 phenomenological approach for the intergranular stresses.

171 **Closure of the intergranular stresses**

172 The intergranular stresses are modelled using the dense granular flows rheology $\mu(I)$
 173 [*Forterre and Pouliquen, 2008; Boyer et al., 2011*] in which the dimensionless number I
 174 can be interpreted as the ratio of a vertical time of rearrangement t_{micro} over a horizontal
 175 time of deformation $t_{macro} = \|\overline{\dot{\gamma}^p}\|^{-1} = |du^p/dz|^{-1}$

$$I = \frac{t_{micro}}{t_{macro}}.$$

176 The microscopic time scale corresponds to the time needed by a particle submitted to
 177 a pressure P^p to fall over its own diameter. Following *Courrech du Pont et al. [2003]* and
 178 *Cassar et al. [2005]* three regimes can be observed : free fall, viscous or turbulent. The
 179 corresponding time scales are given by

$$t_{micro}^{ff} = d_p \sqrt{\frac{\rho_p}{P^p}} ; t_{micro}^v = \frac{\eta_f}{P^p} ; t_{micro}^t = d_p \sqrt{\frac{\rho_f C_D}{P^p}}$$

180 A phase diagram (Figure 2) can be drawn in the plane (St, r) where St is the Stokes
 181 number, defined as the ratio of the free fall time to the viscous one, and r is the ratio of the
 182 free fall time to the turbulent one [*Cassar et al., 2005*]. In the free fall regime the fluid has
 183 no influence on the rheology and the granular media behaves like a dry granular flow. In
 184 the viscous regime, the vertical fall of a particle in the granular assembly is controlled by
 185 the viscous drag. In the turbulent regime, the vertical motion of the particle is controlled
 186 by the turbulent drag.

187 A rough estimate of the characteristic time scales associated to the sheet flow regime
 188 gives the following values of the two above mentioned dimensionless numbers $St \sim 10^{-2} -$
 189 10^2 and $r \sim 10^{-2} - 10^1$ with typical particulate Reynolds number $Re_p = \rho_f w_s d_p / \eta_f \sim$
 190 $10^{-1} - 10^2$ where w_s is the settling velocity of particles. The order of magnitudes used for

191 these estimates are summarized in Table 1. These first estimates show that the granular
 192 flow is potentially at the transition between the three regimes. It is also possible that a
 193 transition occurs within the sheet flow layer itself.

194 In the numerical model, the dimensionless number I is computed as the ratio of the
 195 largest microscopic time scales to the macroscopic one

$$I = \frac{\max(t_{micro}^{ff}, t_{micro}^v, t_{micro}^t)}{t_{macro}}.$$

196 The dense granular flow regime is therefore obtained as a result of the model. This
 197 point will be discussed in detail in subsection 4.1.

198 In the context of a frictional rheology the particulate shear stress is written as

$$\tau_{xz}^p = \mu(I)P^p, \quad (19)$$

199 where the friction coefficient μ depends on the dimensionless number I as a result of
 200 the dimensional analysis. Following the idea originally introduced for dry granular flows
 201 [*GDR midi*, 2004; *Forterre and Pouliquen*, 2008] the same functional form has been used
 202 by *Boyer et al.* [2011] in the viscous regime

$$\mu(I) = \mu_s + \frac{\mu_2 - \mu_s}{I_0/I + 1}, \quad (20)$$

203 where μ_s corresponds to the static friction coefficient or the so-called tangent of the angle
 204 of repose, μ_2 represents a dynamical friction coefficient and I_0 is an empirical parameter
 205 of the rheology.

206 Following *Chauchat and Médale* [2010] a particulate viscosity is defined as

$$\eta_p = \frac{\tau_{xz}^p}{\|\overline{\dot{\gamma}^p}\|} = \frac{\mu(I) P^p}{\|\overline{\dot{\gamma}^p}\|}. \quad (21)$$

207 It should be noted that the particulate viscosity diverges when the particulate shear
 208 rate $\|\overline{\dot{\gamma}^p}\|$ vanishes. This is a typical characteristic of a visco-plastic behaviour of which
 209 the archetype is the Bingham fluid model. The difference between the $\mu(I)$ rheology and
 210 the Bingham one lies in the dependency of the yield stress on the particulate pressure P^p .
 211 With this definition, if the particulate shear rate goes to zero, the particulate viscosity
 212 diverges and the granular media behaves like a solid material. In the numerical model
 213 such divergence raises obvious numerical issues and a regularization technique [*Chauchat*
 214 *and Médale, 2010*] is used

$$\eta_p = \frac{\mu(I) P^p}{\|\overline{\dot{\gamma}^p}\| + \lambda}, \quad (22)$$

215 where λ is the regularization parameter. In the regularized problem, the solid behavior
 216 is replaced by a “very viscous” problem with a viscosity of order $O(\lambda^{-1})$. Consequently, a
 217 creeping flow is predicted by the model in the fixed sediment bed layer. It has been checked
 218 that for all the simulations presented herein, a value of the regularization parameter fixed
 219 to $\lambda = 10^{-6} \text{ s}^{-1}$ guarantee a negligible creeping flow in the fixed bed layer ($z < h_c$).

220 Concentration profile

221 The prediction of the concentration profile is based on the dilatancy law $\phi(I)$ [*Forterre*
 222 *and Pouliquen, 2008; Boyer et al., 2011*]. *Boyer et al.* [2011] have measured precisely this
 223 relationship for volume fractions ranging from 0.4 to 0.585 in the viscous regime and have
 224 proposed the following relationship:

$$\phi(I) = \frac{\phi^m}{1 + I^{1/2}}. \quad (23)$$

225 This formulation allows to describe the asymptotic behavior observed in the experiments
 226 $\phi^m - \phi \propto I^{1/2}$ close to ϕ^m and ensures the positivity of ϕ even for large values of I . It
 227 is also shown that this expression matches the experimental measurements from *Deboeuf*
 228 *et al.* [2009] down to $\phi = 0.3$ for the normal viscosity of dense suspension.

229 From a physical point of view, two quantities control the dilatancy of the granular
 230 media: the particulate pressure and the shear rate. At constant particulate pressure the
 231 concentration decreases when the shear rate increases. This mechanism can be responsible
 232 for the transition between the fixed sediment bed and the dilute suspension in sediment
 233 transport problems.

234 In the present model a similar relationship is used

$$\phi(I) = \frac{\phi^m}{1 + b I^{1/2}}, \quad (24)$$

235 where an additional parameter b , of order unity, has been introduced in order to allow
 236 calibration.

2.2. Boundary layer model in the FL

237 In the FL the horizontal fluid momentum equation reduces to

$$0 = \frac{d\tau_{xz}^f}{dz} + \frac{dR_{xz}^f}{dz} + \rho_f g \sin \beta \quad (25)$$

238 where the presence of suspended particles is neglected both in the gravity and in the
 239 viscous stress terms. The closure for the fluid Reynolds stresses is identical to the SBL

240 one (17)-(18). The mixing length at the bottom of the boundary layer is controlled by
 241 the concentration profile and the thickness in the moving SBL.

242 In the turbulent boundary layer (FL), sediment particles can be suspended by the fluid
 243 turbulence. Following *Rouse* [1937], the suspended concentration profile is determined
 244 from a balance between the settling and the vertical turbulent dispersion fluxes of particles

$$w_s \phi + \frac{\eta_t}{\rho_f} \frac{d\phi}{dz} = 0 \quad (26)$$

245 where w_s represents the settling velocity of sediment particles. This balance equation
 246 can be integrated from a given vertical level at which the volume fraction is known up to
 247 the free surface H . Here the FL/SBL interface is chosen as the reference level.

$$\phi(z) = \phi_{h_p} \exp \left(-\rho_f w_s \int_{h_p}^z \eta_t^{-1} dz \right). \quad (27)$$

248 The validity of the Rouse profile in the suspension above the sheet flow layer has been
 249 demonstrated by *Sumer et al.* [1996]. The authors have shown that the Rouse profile fit
 250 well their data provided that the reference level is taken high enough above the bed, it
 251 should lie in the upper half of the sheet flow layer, that corresponds to typical sediment
 252 concentration of order 0.25.

2.3. Resolution strategy and boundary conditions

253 For the numerical implementation, a pseudo-time integration and an implicit finite
 254 difference discretisation technique are used to compute the steady state solution for both
 255 layers. The FL algebraic system is tridiagonal and is solved using a double sweep algorithm
 256 [*Thomas*, 1995] whereas the SBL two-phase algebraic system is solved using the Moore-
 257 Penrose solver of Matlab®. The problem is decoupled between the two-layers FL and

258 SBL as illustrated in Figure 3. The FL solution gives the bed shear stress applied on the
 259 SBL. In turn the SBL solution gives the boundary conditions for the FL: slip velocity
 260 U_b and sediment volume fraction at the interface ϕ_{h_p} . The mesh in the SBL is updated
 261 once after the FL solution to account for the sediment volume eroded from the SBL, and
 262 second at the end of the SBL solution, after the calculation of ϕ_{SBL} from equation (24).
 263 This latter step account for the bed decompaction. These two mesh adaptations lead to
 264 an error on the sediment volume conservation of less than 0.1 %. More details concerning
 265 the algorithm are given in appendix B.

266 No-slip boundary conditions are imposed for both velocities and the volume fraction is
 267 maximum at the bottom of the SBL (see figure 3). The shear stress is imposed as boundary
 268 condition at the top of the FL (τ_{top} is zero for free surface flows and is computed from the
 269 Colebrook and White formula for duct flows).

270 At the end of the computations the model gives a prediction of the mixture velocity
 271 and the concentration profiles in the whole domain, from the fixed bed up to the free
 272 surface, and the particulate phase velocity profile within the SBL. From this knowledge,
 273 the sediment transport rate $q_p = q_p^{FL} + q_p^{SBL}$ can be computed as

$$q_p^{FL} = \int_{h_p}^H \phi U dz \quad \text{and} \quad q_p^{SBL} = \int_0^{h_p} \phi u^p dz, \quad (28)$$

274 and the sheet flow layer thickness is computed as $\delta_s = h_p - h_c$. The lower limit of the
 275 mobile layer h_c is defined as the vertical position where the concentration has decreased
 276 of 0.1% from the maximum packing fraction.

3. Results

277 The proposed model is used to simulate sheet flow regimes involving two types of sed-
 278 iment over a large range of Shields numbers: $0.5 < \theta < 2.6$. Both sediment types are
 279 taken from sheet flow experiments presented in the literature [*Cowen et al.*, 2010; *Sumer*
 280 *et al.*, 1996] and cover a wide range of properties (Table 2).

281 In subsection 3.1, we focus on the comparison of the vertical flow profiles with *Cowen*
 282 *et al.* [2010]’s and [*Sumer et al.*, 1996]’s experiments. Subsection 3.2 is dedicated to
 283 the study of the macroscopic parameters such as sediment transport rate, mobile layer
 284 thickness and roughness.

3.1. Vertical profiles

285 At first, the model results are compared with two data sets from the literature [*Sumer*
 286 *et al.*, 1996; *Cowen et al.*, 2010] in terms of velocity and concentration profiles. The
 287 physical parameters for these simulations are summarised in Table 2 and 3. The chosen
 288 values of the empirical parameters (κ, μ_2, I_0 and b) are given in Table 4.

289 In the FL, the grid size is geometrically distributed with a reason of 1.048 and a mini-
 290 mum grid size taken as $\Delta z_{min} = \min(0.1 \eta_f / (\rho_f u_*); 0.1 d_p)$ resulting in N_{FL} grid points.
 291 In the SBL, the grid size is distributed following a cosine function refined at both bound-
 292 aries. For all the simulations, the number of grid points N_{SBL} is fixed to 150 that lead to
 293 a minimum grid size smaller than d_p (see Table 4). The pseudo time step is fixed to 10^{-5}
 294 s. These numerical parameters ensures the spatial convergence of the numerical results.

295 Figures 4 (a) and 5 (a) show the numerical velocity profiles compared with *Sumer*
 296 *et al.* [1996]’s and *Cowen et al.* [2010]’s measurements respectively. In the four cases the
 297 simulated velocity profiles present a good agreement with experimental data for different

298 experimental conditions and describe fairly well the transition from the static bed to the
299 mobile sediment layer.

300 In figures 4 (b) and 5 (b), concentration profiles for each experimental conditions are
301 presented. The concentration profile in the SBL is calculated from the dilatancy law
302 $\phi(I)$ (24) whereas it is obtained from the Rouse profile (27) in the FL. The value of the
303 concentration at the top of the SBL is used as the boundary condition for the suspension
304 solution in the FL. This value is in the range $\phi \in [0.2; 0.3]$ that corresponds to the limit
305 value below which the $\phi(I)$ law is valid [Boyer *et al.*, 2011] and above which the Rouse
306 profile fit the experimental measurements [Sumer *et al.*, 1996].

307 In Sumer *et al.* [1996]’s cases, the concentration profile in the dense part of the sheet
308 layer was not measured. The present model results are compared with Hsu *et al.* [2004]’s
309 ones obtained with a two-phase model based on the kinetic theory for the intergranular
310 stresses. It is interesting to note the similarity of the concentration profiles obtained with
311 the dense granular flow rheology and the collisional theory [Hsu *et al.*, 2004]. In both
312 cases the concentration profile exhibits a concentration “shoulder” of a few particles size
313 thickness, characteristic of the existence of a sheet. Both phenomenological rheology and
314 kinetic theory seem to be able to reproduce the existence of this sheet layer. Using γ -ray
315 technique Pugh and Wilson [1999] have measured concentration profiles in a cylindrical
316 geometry that are consistent with the predicted profiles. However, more refined measure-
317 ments are needed to improve our understanding of vertical dispersive mechanisms in the
318 sheet flow layer.

319 Concerning Cowen *et al.* [2010]’s experiment, the transition from the static bed to the
320 sheet flow layer is smoother but the concentration shoulder still exists. However, no

321 experimental data or model results are available in the literature to further assess the
 322 predicted concentration profile. In the FL, the Rouse profile seems to match quite well
 323 with the concentration profile in the SBL. As pointed out by *Sumer et al.* [1996] a Rouse
 324 profile matches the experimental measurements independently from the reference level
 325 chosen provided that the reference concentration is greater than approximately $\phi \approx 0.25$.
 326 This condition is quite well verified in the four cases presented here $\phi_{hp} \in [0.25; 0.3]$. In
 327 the following, we will denote the concentration shoulder as the sheet layer.

328 These first comparisons show that the proposed model is able to simulate quantitatively
 329 the velocity profiles and the concentration profiles for a wide range of Shields number
 330 ($\theta \in [1.25; 2.3]$). It should be noted that the empirical constants of the phenomenological
 331 laws $\mu(I)/\phi(I)$, b and I_0 , are kept constant for both sediment types, A and B. In the
 332 four simulated cases, the concentration in the sheet layer is between $\phi = 0.3$ and $\phi = 0.4$
 333 which is still in the validity domain of the phenomenological rheology [*Boyer et al.*, 2011].
 334 The sensitivity of the model results to the empirical parameters κ , μ_2 , I_0 and b will be
 335 discussed in subsection 4.2.

3.2. Macroscopic parameters

336 In this subsection the macroscopic parameters predicted by the model are compared
 337 to experimental data and empirical correlations from the literature in terms of sediment
 338 transport rate ψ , mobile layer thickness δ_s and roughness k_s . Simulations have been
 339 performed, with the two sediment types A and B, for the following range of Shields
 340 number $\theta \in [0.5; 2.6]$ by varying the bed slope at constant water depth.

341 Figure 6 shows the comparison between the predicted dimensionless sediment transport
 342 rate ψ , the model results from *Hsu et al.* [2004] and the experimental data collected

343 by *Yalin* [1977]. The total load ψ and the bed load contribution ψ^{SBL} are presented
344 to exhibit the qualitative contribution of suspended load for each sediment type. The
345 agreement between the model results and the experiments is rather good. For the light
346 particles, type B, the contribution of the suspended load is much greater than the bed load
347 one. On the contrary, for the massive particles, type A, the suspended load contribution
348 is negligible compared to the bed load one. This observation is consistent with *Sumer*
349 *et al.* [1996]’s phase diagram in the plane $(\theta, w_s/u_*)$. For sediment type A the ratio of the
350 fall velocity over the friction velocity is in the range $w_s/u_* \in [0.74; 1.7]$ whereas it is in
351 the range $w_s/u_* \in [0.32; 0.74]$ for sediment type B. Following *Sumer et al.* [1996]’s phase
352 diagram, sediment type A simulations are mostly in the no suspension mode of sheet flow
353 regime ($w_s/u_* > 1$) whereas sediment type B simulations are all in the suspension mode
354 ($w_s/u_* < 0.8$). The present simulation results are consistent with these observations. It
355 should be mentioned that our results are very close to *Hsu et al.* [2004] ones obtained
356 with a two-phase approach based on kinetic theory of granular flows.

357 Figure 7 shows the comparison between the dimensionless thickness computed with the
358 present model δ_s/d_p , the model results from *Hsu et al.* [2004] and the experimental data
359 reported by *Sumer et al.* [1996]. The comparison shows a fairly good agreement with
360 experimental observations for both models especially for Shields numbers lower than 1.5.
361 For higher Shields numbers, the evolution of the thickness predicted by our model presents
362 a non-linear behaviour for sediment type A that is not observed in the measurements of
363 *Sumer et al.* [1996] or *Hsu et al.* [2004] model results. It should also be pointed out that
364 a significant scatter is observed on the *Sumer et al.* [1996] measurements between visual

365 observations and those deduced from concentration profiles (a factor of two for Shields
366 number between 2 and 3).

367 In order to better understand the influence of the particle properties (shape, density
368 and size), a simple model for the evolution of the thickness versus the Shields number is
369 derived from the mixture momentum balance. This momentum balance is obtained as the
370 sum of the momentum equations for the fluid and the particulate phases (13) and (14),
371 respectively:

$$0 = \frac{dR_{xz}^f}{dz} + \frac{d\tau_{xz}^f}{dz} + \frac{d\tau_{xz}^p}{dz} + \rho_m g \sin \beta, \quad (29)$$

372 where $\rho_m = \epsilon \rho_f + \phi \rho_p$ is the mixture density. This equation can then be integrated
373 between a given vertical position z in the SBL and the FL/SBL interface h_p , as follows:

$$R_{xz}^f(z) + \tau_{xz}^f(z) + \tau_{xz}^p(z) = \tau_b + g \sin \beta \int_z^{h_p} \rho_m(z) dz, \quad (30)$$

374 where it is assumed that the intergranular stresses vanishes at the FL/SBL interface
375 $\tau_{xz}^p(h_p) = 0$ and $\tau_b = R_{xz}^f(h_p) + \tau_{xz}^f(h_p)$ represents the total fluid bed shear stress.

376 We then introduce the mean sheet flow layer concentration $\bar{\phi}$, defined as: $\bar{\phi} \delta_s =$
377 $\int_{h_c}^{h_p} \phi(z) dz$. Using this notation, the integral in the RHS of equation (30) can be rewritten
378 as:

$$\int_{h_c}^{h_p} \rho_m(z) dz = \delta_s [\rho_f + (\rho_p - \rho_f)\bar{\phi}]. \quad (31)$$

379 Furthermore, at the location of the boundary between the stationary and moving sedi-
380 ment ($z = h_c$), we can assume that the mixture stresses are dominated by the intergranular
381 ones, *i.e.* the fluid stresses are negligible. This assumption will be justified in subsection

382 4.3. The velocity profiles presented in figure 4 and 5 show that the shear rate goes to
 383 zero there. Consequently, the parameter I also vanishes and $\tau_{xz}^p(h_c) = \mu_s p^p(h_c)$ which
 384 is a classical Coulomb yield criterion [*Hanes and Inman, 1985*]. With these assumptions
 385 and the hydrostatic particulate pressure distribution (12), equation (30) can be rewritten
 386 between h_c and h_p in dimensionless form:

$$\frac{\delta_s}{d_p} = \frac{\theta}{\mu_s \bar{\phi} \cos \beta - [\rho_f / (\rho_p - \rho_f) + \bar{\phi}] \sin \beta}. \quad (32)$$

387 For sufficiently small inclination angles, *i.e.* $\sin \beta \ll \cos \beta \approx 1$, one obtains the
 388 following simple relationship for the thickness of the sheet flow layer:

$$\frac{\delta_s}{d_p} = \frac{\theta}{\mu_s \bar{\phi}}. \quad (33)$$

389 These two last expressions are identical to equation (3.16) presented by *Ouriemi et al.*
 390 [2009] in the laminar case in which the longitudinal pressure gradient replaces the gravity
 391 term. The simplified model, equation (33), is similar to the one obtained by *Wilson* [1987],
 392 inspired from *Bagnold* [1956], with the difference that the friction coefficient here is the
 393 static one and not the dynamical one. In figure 7 the predictions obtained with equations
 394 (32) and (33) together with the one from *Wilson* [1987]’s model are presented. For sedi-
 395 ment types A and B, the predictions obtained using equation (32) are in good agreement
 396 with the full numerical solution. The slight overestimation of the dimensionless thickness,
 397 less than 5%, is induced by the regularization technique in a non-trivial way. Prediction
 398 obtained with (33) is a good approximation of (32) as far as the gravity term is negligible
 399 compared with the fluid bed shear stress and friction ones. This is the case for the “light
 400 particles” (type B) for which the proposed model and *Wilson* [1987]’s model are in good

401 agreement. On the contrary, for the “massive particles” (type A) the gravity term is not
402 negligible and a variation of as much as 100% is observed between the simplified model
403 (33) and the complete one (32). One should keep in mind that gravity effects can become
404 significant for “massive particles” that are not accounted for in simplified relationships
405 such as (33) or *Wilson* [1987]’s model. For example, the simulations performed in this
406 paper suggest that this is the case in *Sumer et al.* [1996]’s experiments.

407 The difference between sediment type A and B shows an influence of the particles
408 frictional properties: sediment type A, that are not spherical, exhibits a higher static
409 friction coefficient ($\mu_s = 0.51$) than the glass beads (sediment type B ; $\mu_s = 0.3$). This
410 influence is captured by the simplified model (33), however it is screened by the influence of
411 gravity. Further works are needed to better understand the role of the particle properties
412 in sheet flow regime (shape, size and density).

413 In figure 8 the evolution of the dimensionless roughness versus the Shields number is
414 presented. In the present model the roughness is obtained from the value of the mixing
415 length at the FL/SBL interface $k_s = l_m(h_p)$. This definition is consistent with our mixing
416 length approach where its value at the interface represents the more energetic eddies
417 length scale within the sheet flow layer. It is interesting to note that the roughness non-
418 dimensionalized by the thickness of the sheet layer is rather constant with the Shields
419 number independently of the sediment types. This characteristic has been observed by
420 *Grant and Madsen* [1982], *Nnadi and Wilson* [1992] and *Hsu et al.* [2004], amongst others,
421 and is well reproduced by the present model.

422 It appears from these three comparisons that the dense granular rheology allows to
423 correctly predict the main features of the sheet flow regime.

4. Discussion

In this section the model results are analysed and discussed. First, the dense granular rheology regime(s) encountered in the sheet flow regime are deduced from the model results. Second, the sensitivity of the model solution to the phenomenological parameters is presented. Third, the stresses repartition in the sheet flow layer are discussed and the vertical distribution of the sediment transport flux are analysed. Finally, a discussion on the main limitations of both the kinetic theory of dense granular flows and the dense granular rheology for application to sheet flow regime is presented.

4.1. Dense granular rheology regimes

As mentioned in the model formulation (section 2), the sheet flow regime of sediment transport is at the transition between viscous, free fall and turbulent regimes of the granular rheology. The phase diagram presented in Figure 2 allows to represents graphically these regimes. As explained previously, the competition between the three time scales associated with the vertical motion of a particle in the granular assembly leads to the three above mentioned regimes:

• **Viscous regime:** $t_{micro}^v \gg t_{micro}^{ff} ; t_{micro}^t$.

i.e. $St \ll 1$ and $r \gg St$

• **Free fall regime:** $t_{micro}^{ff} \gg t_{micro}^v ; t_{micro}^t$.

i.e. $St \gg 1$ and $r \gg 1$

• **Turbulent regime:** $t_{micro}^t \gg t_{micro}^v ; t_{micro}^{ff}$.

i.e. $St \gg r$ and $r \ll 1$

In figure 9 the values of the Stokes number and the r number, for each grid point in the SBL and for all the simulations performed (*i.e.* for all Shields numbers), are plotted. As

445 expected most of the points are close to the transition. For all but a few points the Stokes
446 number is greater than unity, hence the particles vertical motion is hardly affected by the
447 fluid viscosity in the sheet flow regime. For the lighter particles most of the points are in
448 the turbulent regime $r < 1 < St$ except at the FL/SBL interface. The particles inertia
449 does not control the vertical time scale of rearrangement for sediment type B and fluid
450 turbulence is expected to be the control mechanism in the sheet flow layer. However, for
451 sediment type A all the points are in the free fall regime, the grain inertia dominate the
452 time scale of rearrangement, like in the dry granular case.

453 *Ouriemi et al.* [2009], *Aussillous et al.* [2012] and *Boyer et al.* [2011] have shown that
454 the $\mu(I)$ rheology is able to describe fairly well the granular flow in the viscous regime
455 for different configurations. The agreement between the present model results and the
456 experimental data from *Cowen et al.* [2010] (sediment type B) gives some clues that the
457 granular rheology could be relevant in the turbulent regime as well. The authors are not
458 aware of any publications concerning such application of the dense granular rheology in
459 this regime.

460 It is interesting to note that the predicted regimes of the dense granular rheology are
461 consistent with the picture existing in the literature concerning the dominant mechanisms
462 acting in the sheet flow regime: collisional interactions for massive particles, corresponding
463 to the free fall regime, and fluid velocity fluctuations for light particles, corresponding
464 to the turbulent regime. The phenomenological rheology seems to be able to capture
465 intrinsically the transition between those two mechanisms.

4.2. Sensitivity analysis

466 The proposed model introduces several phenomenological parameters (κ , μ_2 , I_0 and
 467 b , see Table 4). In the following, the chosen parameter values are discussed in light of
 468 previous works and a sensitivity analysis for the two parameters I_0 and b is presented.

469 The value of the Von Karman “constant” has been fixed to 0.35 for sediment type A and
 470 0.41 for sediment type B by comparison with experimental data. It has been suggested by
 471 *Vanoni* [1975] and *Amoudry et al.* [2008], amongst others, that the presence of sediment
 472 particles can lead to a reduction of the Von Karman constant. For example, *Longo* [2005]
 473 found values in the range 0.33 to 0.38 for sand sheet flows. In order to quantify the
 474 sensitivity to the Von Karman constant, we have performed simulations for *Sumer et al.*
 475 [1996]’s experiments with $\kappa = 0.41$, in place of 0.35, and have found relative variations of
 476 the sediment transport rate of 8%, 2.5% and 2.3% for runs 82, 91 and 99, respectively. The
 477 relative variation for the sheet flow layer thickness is negligible (less than 1.5%). Therefore
 478 the macroscopic parameters predicted by the model are not so sensitive to variations of
 479 the Von Karman constant.

480 As stated in *Pouliquen* [1999] and [*Forterre and Pouliquen*, 2008], the parameter μ_2
 481 is intrinsic to the particles type (material and shape) and corresponds to the tangent of
 482 the maximum angle below which a steady uniform flow is possible in gravity driven flows
 483 down an inclined plane. From comparison with experiments, we have calibrated $\mu_2 = 0.7$
 484 for sediment type A and $\mu_2 = 0.64$ for sediment type B. These values are coherent with
 485 the ones presented in the literature [*Forterre and Pouliquen*, 2008; *Boyer et al.*, 2011].

486 It follows that I_0 and b are the only two purely phenomenological parameters of the
 487 proposed model. The chosen value for I_0 is identical to the one used for dry granular flows
 488 in the inertial regime, *e.g.* *Forterre and Pouliquen* [2008]. In figure 10 the sensitivity of

489 the model results to the parameters I_0 and b is presented for the *Sumer et al.* [1996]'s
 490 experiments. Values of I_0 between 0.1 and 1 and b between 0.5 and 1 have been tested and
 491 the relative variation of the dimensionless sediment transport rate $\Delta\psi/\psi^{ref}$ and of the
 492 thickness $\Delta\delta_s/\delta_s^{ref}$ are presented. Where ψ^{ref} and δ_s^{ref} correspond to the reference results
 493 obtained with the original values of the parameters ($I_0 = 0.3$ and $b = 0.75$). It is observed
 494 that I_0 has no significant influence on the thickness ($\leq 5\%$) and the sediment transport
 495 rate shows maximum relative variation of 25%. The parameter b has less influence on
 496 the sediment transport rate, with typical relative variations of about $\pm 15\%$ and more
 497 influence on δ_s than I_0 ($\approx \pm 15\%$). It is also observed that δ_s is an increasing function of
 498 I_0 and b whereas ψ is an increasing function of I_0 and a decreasing function of b . From this
 499 sensitivity analysis we can deduce that I_0 , the phenomenological parameter of the $\mu(I)$
 500 law, has mainly an influence on the velocity profile and not much on the concentration one.
 501 On the contrary b , that only appears in the dilatancy law $\phi(I)$, has mainly an influence
 502 on the thickness. As a conclusion, the relatively small sensitivity of the model results to
 503 the phenomenological parameters, I_0 and b , demonstrates the robustness of the model.

4.3. Stresses and sediment flux repartition

504 Figure 11 shows the mixture stresses repartition in the SBL as given by (30). In the
 505 lower part of the sheet flow layer, where the concentration is close to the maximum
 506 packing fraction, the intergranular stresses dominate. Upper in the sheet flow layer, the
 507 intergranular stresses decrease and the fluid ones increase. At a given point, the fluid
 508 stresses and the intergranular ones match. This point is located around the two third of
 509 the sheet layer thickness. This was also observed by *Hsu et al.* [2004] in their two-phase
 510 model based on the kinetic theory of granular flows. In the concentration shoulder, both

511 intergranular stresses and fluid Reynolds stresses are of the same order of magnitude.
512 Above the concentration shoulder, the fluid Reynolds stresses dominate the mixture ones,
513 consistently with the transition toward the suspension. In the whole domain, the relative
514 contribution of the viscous stresses compared with the total fluid stresses are negligible
515 except in a very thin layer near the bottom of the sheet flow layer. However, in this
516 region the fluid stresses are negligible compared with the intergranular ones. Therefore,
517 the contribution of the viscous stresses are not significant to this problem. This confirms
518 the conclusion deduced from the analysis of the dense granular flow rheology regimes
519 presented in subsection 4.1.

520 From a conceptual point of view the SBL can be split into three layers: the upper layer,
521 dominated by the fluid turbulence; the middle layer, corresponding to the concentration
522 shoulder where the Reynolds stresses and the intergranular ones have the same order of
523 magnitudes and the lower layer, dominated by the particle-particle interactions. In *Berzi*
524 [2011]’s model, a macro-viscous layer is considered at the bottom where the fluid-particle
525 mixture behaves as a viscous suspension. The collisional layer is splitted into two parts,
526 a dense algebraic layer, in which an equilibrium between production of fluctuating energy
527 and dissipation due to collisions is assumed, and a diffuse collisional layer, in which the
528 balance of particle fluctuation energy is solved using the trapezium rule. The lower layer of
529 the proposed model and the macro-viscous one from *Berzi* [2011]’s model are physically
530 consistent. However, in the collisional layer, *Berzi* [2011] neglects the fluid Reynolds
531 stresses whereas in the upper layer of the proposed model, the intergranular stresses are
532 negligible. Therefore, improvements of both approaches requires a better understanding
533 of the complex interactions between fluid turbulence and collisions (four-way coupling).

534 It should also be pointed out that the concentration in this layer is obtained solely from
 535 the dilatancy law $\phi(I)$ and turbulent dispersion effects are neglected. Due to dominant
 536 fluid Reynolds stresses in the upper part of the SBL this assumption is probably too
 537 strong. If this effect was accounted for, the concentration would be lower in this region
 538 and the concentration profiles would be closer to the ones predicted by *Hsu et al.* [2004]’s
 539 model (see figure 4).

540 The vertical distribution of the horizontal sediment flux $\pi = \phi u^p$ is presented in figure 12
 541 in order to determine the most efficient region for the sediment transport. The maximum
 542 of the flux is located at the SBL/FL interface ($\phi \approx 0.25 - 0.3$). The curves of the
 543 cumulative flux ($\Pi = \int_0^z \pi(\xi) d\xi$) show that different behaviors are observed for the two
 544 sediment types. With sediment type A [*Sumer et al.*, 1996], the sheet layer contributes
 545 to 65% of the total solid load, while for sediment type B [*Cowen et al.*, 2010], the sheet
 546 layer contributes only to 15% of the total solid load. As discussed in subsection 3.2
 547 this is consistent with the phase diagram presented in *Sumer et al.* [1996]. The ratio of
 548 the fall velocity over the friction velocity controls the importance of the suspended load.
 549 Sediment type A has a ratio between 0.74 and 1.7 whereas sediment type B has a ratio
 550 between 0.32 and 0.74. Following *Sumer et al.* [1996], the transition between the no-
 551 suspension mode and the suspension mode of sheet flow is observed for a ratio lower than
 552 0.8. Therefore, for “massive particles” ($w_s/u_* \geq 0.8$) the description of the SBL is critical
 553 to the prediction of the sediment transport flux. The dense granular rheology is shown
 554 to correctly predict the granular behavior in the sheet flow regime. For “light particles”
 555 ($w_s/u_* \leq 0.8$), the existence of a mobile sheet layer is associated to a high suspended load.
 556 It is essential to correctly describe the transition from the static bed to the suspension

557 in order to get quantitative predictions of the sediment transport characteristics. The
558 present model seems to be also relevant for this purpose however more precise validations
559 against experimental data are needed.

4.4. Dense granular rheology versus kinetic theory

560 In this last subsection, we discuss the limitations and advantages of both the kinetic
561 theory and the dense granular rheology.

562 Originally the kinetic theory has been developed to describe the gaseous regime of
563 granular flows. It is based on the assumption of uncorrelated, instantaneous and binary
564 collisions [*Jenkins and Richman*, 1985] that is not verified when the particle response
565 time is shorter than the fluid one (small Stokes number) and in dense shearing flows,
566 when repeated collisions and/or enduring contacts between the particles occur [*Jenkins*,
567 2006, 2007].

568 Concerning the influence of the ambient fluid two mechanisms can modify the collisional
569 interactions. First, when the particle inertia is so small that collisions are damped by the
570 fluid viscosity [*Berzi*, 2011]. Second, when the particle response time is small compared
571 with the fluid turbulent one the particles follow closely the fluid velocity fluctuations and
572 the collisions can not be considered as uncorrelated. *Hsu et al.* [2004] proposed a mixing
573 length that depends on the Stokes number to account for this phenomenon.

574 Mainly three approaches have been proposed to modify the original kinetic theory to
575 account for enduring contacts [*Forterre and Pouliquen* [2008] and references therein].
576 First, a frictional stress term can be added to the collisional one (*e.g.* *Johnson and Jackson*
577 [1987]). Second, the transport coefficients of the kinetic theory can be modified in the
578 region of enduring contacts (*e.g.* *Kumaran* [2006]). A last idea postulates the existence

579 of a length scale larger than the particle diameter related to the formation of clusters
580 [*Jenkins*, 2006]. In order to describe the transition between the gaseous and the liquid
581 regimes, Hsu and co-workers (*e.g.* *Hsu et al.* [2004]) have introduced a modification of the
582 radial distribution function and an additional closure for the particle pressure to account
583 for enduring contacts. *Berzi* [2011], in his analytical solution of sheet flow, has used the
584 same approach to describe the liquid regime (macro-viscous layer) and has accounted for
585 multiple and repeated collisions using the correlation length proposed by Jenkins and
586 co-worker (*e.g.* *Jenkins* [2006]). However, as stated by the authors, this extension is
587 not meant to apply when enduring contacts dominate. It should also be noted that, in
588 these models, the constitutive equations of the kinetic theory have been modified in a
589 phenomenological way.

590 Concerning the dense granular rheology, the following limitations applies to the mod-
591 elling of sheet flow. First, no fundamental theory exists to link the form of the friction
592 and dilatancy laws to the microscopic properties of the particles (*e.g.* restitution coef-
593 ficient, shape, particle friction coefficient). Second, the hysteretic character of the flow
594 threshold are not accounted for. Third, the phenomenological approach can not capture
595 the gaseous regime of granular flows. This regime falls in the framework of the kinetic
596 theory. Besides that, the results presented in this paper shows that the dense granular
597 rheology coupled with the mixing length approach for the fluid Reynolds stresses allows
598 to describe the sheet flow regime. Furthermore, as shown in the discussion on rheology
599 regimes (subsection 4.1), the dense granular rheology potentially captures the transition
600 between collisional dominant and fluid velocity fluctuations dominant sheet flow regime.

601 From this short discussion it appears clearly that both the kinetic theory and the phe-
602 nomenological approach have some limitations concerning the modelling of sheet flow.
603 The original kinetic theory is not appropriate in the dense part of the sheet flow whereas
604 the phenomenological approach is not appropriate for dilute conditions *a priori*. However,
605 as illustrated in figures 6 and 7, both approaches are shown to be able to quantitatively
606 predict the main features of the sheet flow provided that constitutive laws are cautiously
607 calibrated against experimental measurements. The proposed model can be considered
608 as an alternative approach to the Bagnold's law and to the kinetic theory for modeling
609 intergranular stresses. One of the advantage of the proposed model compared with kinetic
610 theory ones is that no additional transport equations, with complex boundary conditions,
611 have to be solved. However some specific numerical techniques must be used to deal with
612 the visco-plastic behavior of the dense granular rheology.

5. Summary and conclusion

613 An original two-phase model for sheet flow regime based on recent advances in dense
614 granular flows has been presented. Using the dense granular rheology $\mu(I)$ and dilatancy
615 law $\phi(I)$ coupled with a mixing length approach, the model has been validated against
616 experimental data for the velocity profiles. The concentration profiles, for which no mea-
617 surements are available, are consistent with those obtained by kinetic theory of granular
618 flows. The evolution of the sheet flow macroscopic parameters such as sediment trans-
619 port rate, thickness and roughness, against Shields parameter are in good agreement with
620 existing experimental data and empirical correlations.

621 The main conclusions of the present paper can be summarized as follows:

622 i) The transition between collisional and fluid turbulent dominant sheet flow is captured
623 by the dense granular rheology depending on the particles characteristics and the local
624 shear rate. This transition is characterized by a transition between the turbulent regime
625 for “light particles” and the free fall one for “massive particles”. In sheet flow regime,
626 “massive particles” behaves like a dry granular flow meaning that the fluid has a negligible
627 influence.

628 ii) The robustness of the model has been demonstrated from a sensitivity analysis per-
629 formed for the two purely empirical parameters of the dense granular rheology (I_0 and b).
630 For variations of these two parameters as high as 300% the model solution only varies in
631 a range of less than 25%.

632 iii) A layer decomposition based on an analysis of the stresses repartition inside the
633 sheet flow layer, is proposed:

634 – A dense frictional layer with dominant intergranular stresses that describes the
635 transition to the static bed.

636 – A sheet layer where intergranular stresses and turbulent stresses are of the same
637 order of magnitude.

638 – A turbulent dilute region with dominant turbulent stresses that describes the tran-
639 sition to the suspension.

640 iv) From a practical point of view, the proposed model predicts a maximum of the
641 sediment flux at the top of the sheet flow layer for both massive and light particles. For
642 massive particles most of the flux occurs in the moving bed layer whereas for the light
643 particles most the flux occurs in the suspension layer.

644 As a general conclusion, it has been demonstrated that the dense granular rheology
 645 $(\mu(I)/\phi(I))$ can be used as an alternative approach to the kinetic theory of granular flow
 646 for modeling intergranular stresses in two-phase model for sheet flow regime.

647 In future work, a more refined turbulence model should be introduced to improve the
 648 modeling of the fluid particles turbulent interactions (two-way and four-way coupling).
 649 Further works are also needed to better understand the influence of the particles char-
 650 acteristics (shape, density, size, ...) on the dominant mechanisms acting in sheet flow
 651 regime. We strongly believe that higher resolution experimental data inside the sheet
 652 flow layer are needed to further improves theoretical models.

Appendix A: Summary of the model equations

653 The numerical model is based on the resolution of the following set of ordinary differ-
 654 ential equations using an impicite finite difference method. The two layers are solved
 655 alternatively the FL solution gives an estimate of the shear stress acting on the SBL
 656 whereas the FL solution gives an estimate of the slip velocity for the FL.

657 Boundary layer model in the FL

$$0 = \frac{d}{dz} \left[(\eta_f + \eta_t) \frac{du^f}{dz} \right] + \rho_f g \sin \beta \quad (\text{A1})$$

658 Two-phase model in the SBL

$$0 = \frac{d}{dz} \left[\eta_p \frac{du^p}{dz} \right] + \phi \frac{d}{dz} \left[(\eta_e + \eta_t) \frac{dU}{dz} \right] \quad (\text{A2})$$

$$+ C_D (U - u^p) + \phi \rho_p g \sin \beta$$

$$0 = (1 - \phi) \frac{d}{dz} \left[(\eta_e + \eta_t) \frac{dU}{dz} \right] \quad (\text{A3})$$

$$-C_D (U - u^p) + (1 - \phi) \rho_f g \sin \beta$$

$$\phi = \frac{\phi^m}{1 + b I^{1/2}} \quad (\text{A4})$$

$$0 = + \frac{dP^f}{dz} + \rho_f g \cos \beta \quad (\text{A5})$$

$$0 = - \frac{dP^p}{dz} - \phi(\rho_p - \rho_f) g \cos \beta$$

Appendix B: Numerical algorithm

659 Initialisation: k=0

660

661 $U_{FL}^0 = 0$

662 $U_{SBL}^0 = 0$; $u^p{}^0 = 0$ and $p^p = \phi^m \Delta \rho g (h_p - z^0)$

663 $\tau_b^f{}^0 = 0$ and $U_b^0 = 0$.

664 $k = k + 1$

665

666 **Step 1:** U_{FL}^{k+1} is obtained by solving (25) with bottom boundary conditions:

$$(\eta + \eta_t) \frac{dU_{SBL}^{k+1}}{dz} \Big|_{z=H} = \tau_{fs}$$

667 and

$$U_{FL}^{k+1} \Big|_{z=h_p} = U_b^k$$

668 This solution gives the fluid bed shear stress $\tau_b^{f, k+1}$.

669

670 **Step 2:** ϕ_{FL}^{k+1} is obtained from (27) and the suspended volume of sediment is given by:

$$V_{FL}^{k+1} = \int_{h_p^k}^H \phi_{FL}^{k+1} dz.$$

671

672

673 **Step 3:** The space step in each cell is updated to ensures the total volume conservation:

$$dz_j^* = dz_j^k + \frac{V_{FL}^{k+1} - V_{FL}^k}{\phi_{SBL}^k (N_{SBL} - 1)}$$

674 The volume conservation reads:

$$V_{FL}^{k+1} + V_{SBL}^* = V_{FL}^k + V_{SBL}^k$$

675 with $V_{SBL}^* = \int_0^{h_p^*} \phi_{SBL}^k dz$ and $V_{SBL}^k = \int_0^{h_p^k} \phi_{SBL}^k dz$.

676

677 **Step 4:** P^p the particulate pressure is updated after the remeshing of the SBL grid:

$$P^p(z) = \Delta \rho g \int_z^{h_p^*} \phi_{SBL}^k dz.$$

678

679

680 **Step 5:** U_{SBL}^{k+1} and $u^{p\ k+1}$ are obtained by solving (13)-(14) with boundary conditions:

$$(\eta + \eta_t) \frac{dU_{SBL}^{k+1}}{dz} \Big|_{z=h_p} = \tau_b^{f\ k+1}$$

681 and

$$U_{SBL}^{k+1} \Big|_{z=0} = u_{SBL}^{p\ k+1} \Big|_{z=0} = 0.$$

682 This solution gives the value of the boundary condition in the FL: $U_b^{k+1} = U_{SBL}^k \Big|_{z=h_p}$.

683

684 **Step 6:** ϕ_{SBL}^{k+1} is obtained from (24). This solution gives the value of the boundary con-
 685 dition in the FL: $\phi_{h_p}^{k+1} = \phi_{SBL}^{k+1} \Big|_{z=h_p}$.

686

687

688 **Step 7:** z_j^{k+1} is updated to ensure mass conservation in each cell j: $dz_j^{k+1} \phi_{SBL\ j}^{k+1} =$
 689 $dz_j^k \phi_{SBL\ j}^k$.

690

691 This coupling procedure (step 1 to step 7) is iterated until convergence is reached for the
 692 two quantities τ_b^k and U_b^k with typical relative residual of 10^{-5} . Also a convergence criteria
 693 of 10^{-6} on the relative residual for the velocities in Root Mean Square norm is imposed
 694 for both layers. Step 3 ensures the mass conservation in the whole domain whereas step 7

695 ensures mass conservation in the SB layer due to the shear induced decompaction of the
696 sediment bed. A shear stress at the free surface τ_{fs} can be imposed to model the presence
697 of a roof. It is calculated from the Colebrook and White formula.

698 **Acknowledgments.**

699 The authors acknowledge the DGA for the financial support of the first author PhD
700 Thesis (N° 2011-170914/DGA/DS/MRIS) and the LEGI for its financial support. The
701 authors also acknowledge P. Aussillous, Y. Forterre, E. Guazzelli and O. Pouliquen for the
702 fruitful discussions concerning the physics of dense granular flows and the phenomenolog-
703 ical rheology, Daniel Lhuilier for the fruitfull discussions concerning the two-phase model
704 and N. Delgado for the contribution to the model development during its Master degree.
705 The Associate editor and the two anonymous reviewers constructive comments has been
706 greatly appreciated during the review process.

References

- 707 Amoudry, L., T. J. Hsu, and P. L. F. Liu, Two-phase model for sand transport in sheet
708 flow regime, *J. Geophys. Res.*, *113*, 2008.
- 709 Andreotti, B., Y. Forterre, and O. Pouliquen, *Les milieux granulaires entre fluide et solide*,
710 CNRS edition, 2011.
- 711 Aussillous, P., J. Chauchat, M. Pailha, M. Médale, and E. Guazzelli, Investigation of the
712 mobile granular layer in bed-load transport, *Journal of Fluid Mechanics, Submitted*,
713 2012.
- 714 Bagnold, R. A., Experiments on a gravity-free dispersion of large solid spheres in a new-
715 tonian fluid under shear, *Phil. Trans. R. Soc. Lond.*, *225*, 49–63, 1954.

- 716 Bagnold, R. A., The flow of cohesionless grains in fluids, *Phil. Trans. R. Soc. Lond.*, *249*,
717 235–297, 1956.
- 718 Berzi, D., Analytical solution of collisional sheet flows, *Journal of Hydraulic Engineering*,
719 *137*(10), 1200–1207, 2011.
- 720 Bombardelli, F., and S. Jha, Hierarchical modeling of the dilute transport of suspended
721 sediment in open channels, *Environmental Fluid Mechanics*, *9*, 207–235, 2009.
- 722 Boyer, F. m. c., E. Guazzelli, and O. Pouliquen, Unifying suspension and granular rheol-
723 ogy, *Phys. Rev. Lett.*, *107*, 188,301, doi:10.1103/PhysRevLett.107.188301, 2011.
- 724 Cassar, C., M. Nicolas, and O. Pouliquen, Submarine granular flows down inclined planes,
725 *Physics of Fluids*, *17*(10), 103301, doi:10.1063/1.2069864, 2005.
- 726 Chauchat, J., and M. Médale, A 3D numerical model for incompressible two-phase flow
727 of a granular bed submitted to a laminar shearing flow, *Computer Methods in Applied*
728 *Mechanics and Engineering*, *199*, 439–449, 2010.
- 729 Courrech du Pont, S., P. Gondret, B. Perrin, and M. Rabaud, Granular avalanches in
730 fluids, *Phys. Rev. Lett.*, *90*, 044,301, 2003.
- 731 Cowen, E. A., R. D. Dudley, Q. Liao, E. A. Variano, and P. L.-F. Liu, An insitu borescopic
732 quantitative imaging profiler for the measurement of high concentration sediment ve-
733 locity, *Experiments in Fluids*, *49*(1), 77–88, 2010.
- 734 Deboeuf, A., G. Gauthier, J. Martin, Y. Yurkovetsky, and J. F. Morris, Particle pressure
735 in a sheared suspension: A bridge from osmosis to granular dilatancy, *Phys. Rev. Lett.*,
736 *102*, 108,301, doi:10.1103/PhysRevLett.102.108301, 2009.
- 737 Dong, P., and K. Zhang, Two-phase flow modelling of sediment motions in oscillatory sheet
738 flow, *Coastal Engineering*, *36*(2), 87 – 109, doi:DOI: 10.1016/S0378-3839(98)00052-0,

- 1999.
- 739
- 740 Forterre, Y., and O. Pouliquen, Flows of dense granular media, *Annual Review of Fluid*
741 *Mechanics*, *40*, 1–24, doi:10.1146/annurev.fluid.40.111406.102142, 2008.
- 742 Gao, P., Transition between two bed-load transport regimes: Saltation and sheet flow,
743 *Journal of Hydraulic Engineering*, *134*(3), 340–349, 2008.
- 744 GDR midi, On dense granular flows, *The European Physical Journal E*, *14*, 341–365, 2004.
- 745 Gilbert, G. K., The transportation of debris by running water, *Tech. Rep. 86*, USGS
746 Professional Paper, 1914.
- 747 Grant, W. D., and O. S. Madsen, Movable bed roughness in unsteady oscillatory flow, *J.*
748 *Geophys. Res.*, *87*(C1), 469–481, 1982.
- 749 Greimann, B., and F. Holly, Two-phase flow analysis of concentration profile, *J. Hydraulic.*
750 *Eng.- ASCE*, *127*, 753 – 761, 2001.
- 751 Hanes, D. M., and A. J. Bowen, A granular-fluid model for steady intense bed-load trans-
752 port, *J. Geophys. Res.*, *Vol. 90*, 1985.
- 753 Hanes, D. M., and D. L. Inman, Experimental evaluation of a dynamic yield criterion for
754 granular fluid flows, *J. Geophys. Res.*, *90*(B5), 3670–3674, 1985.
- 755 Hsu, T., J. T. Jenkins, and L. F. Liu, On two-phase sediment transport: Dilute flow, *J.*
756 *Geophys. Res.*, *108*, 14, 2003.
- 757 Hsu, T.-J., J. T. Jenkins, and P. L.-F. Liu, On two-phase sediment transport: sheet flow of
758 massive particles, *Proceedings of the Royal Society of London. Series A: Mathematical,*
759 *Physical and Engineering Sciences*, *460*(2048), 2223–2250, doi:10.1098/rspa.2003.1273,
760 2004.

- 761 Jackson, R., *The dynamics of fluidized particles*, Cambridge University Press, Cambridge,
762 2000.
- 763 Jenkins, J. T., Dense shearing flow of inelastic disks, *Physics of Fluids*, 18, 393–410,
764 doi:10.1063/1.2364168, 2006.
- 765 Jenkins, J. T., Dense inclined flow of inelastic spheres, *Granular matter*, 10, 47–52, doi:
766 10.1007/s10035-007-0057-z, 2007.
- 767 Jenkins, J. T., and D. M. Hanes, Collisional sheet flows of sediment driven by a turbulent
768 fluid, *Journal of Fluid Mechanics*, 370(-1), 29–52, doi:null, 1998.
- 769 Jenkins, J. T., and M. W. Richman, Grad’s 13-moment system for a dense gas of inelastic
770 spheres, *Archive for Rational Mechanics and Analysis*, 87, 355–377, 1985.
- 771 Johnson, P. C., and R. Jackson, Frictional-collisional constitutive relations for granular
772 materials, with application to plane shearing, *Journal of Fluid Mechanics*, 176, 67–93,
773 1987.
- 774 Krieger I.M., and Dougherty T.J., A mechanism for non-Newtonian flow in suspensions
775 of rigid spheres, *T. Soc. Rheol.*, 3, 137-157, 1959.
- 776 Kumaran, V., The constitutive relation for the granular flow of rough particles, and its
777 application to the flow down an inclined plane, *Journal of Fluid Mechanics*, 561, 1–42,
778 2006.
- 779 Li, and Sawamoto, Multi-phase model on sediment transport in sheet-flow regime under
780 oscillatory flow, *Coastal engineering Japan*, 38, 157–178, 1995.
- 781 Longo, S., Two-phase flow modeling of sediment motion in sheet-flows above plane
782 beds, *Journal of Hydraulic Engineering*, 131(5), 366–379, doi:10.1061/(ASCE)0733-
783 9429(2005)131:5(366), 2005.

- 784 Meyer-Peter, E., and R. Muller, Formulas for bed-load transport, in *2nd Meeting of the*
785 *International Association of Hydraulic and Structural Research*, pp. 34–64, 1948.
- 786 Nnadi, F. N., and K. C. Wilson, Motion of contact-load particles at high shear stress,
787 *Journal of Hydraulic Engineering*, 118(12), 1670–1684, doi:10.1061/(ASCE)0733-
788 9429(1992)118:12(1670), 1992.
- 789 Ouriemi, M., P. Aussillous, and E. Guazzelli, Sediment dynamics. Part I: Bed-load trans-
790 port by shearing flows, *Journal of Fluid Mechanics*, 636, 295–319, 2009.
- 791 Pouliquen, O., Scaling laws in granular flows down rough inclined planes, *Physics of*
792 *Fluids*, 11(3), 542–548, doi:10.1063/1.869928, 1999.
- 793 Pugh, F. J., and K. C. Wilson, Velocity and concentration distributions in sheet flow
794 above plane beds, *Journal of Hydraulic Engineering*, 125(2), 117–125, 1999.
- 795 Richardson, J. F., and W. N. Zaki, Sedimentation and fluidization: Part i, *Trans. Instn.*
796 *Chem. Engrs*, 32, 1954.
- 797 Rouse, H., Modern conceptions of the mechanics of turbulence, *Trans. Am. Soc. Civ.*
798 *Eng.*, 102, 463 – 505, 1937.
- 799 Sumer, B. M., A. Kozakiewicz, J. F. e, and R. Deigaard, Velocity and concentration
800 profiles in sheet-flow layer of movable bed, *Journal of Hydraulic Engineering*, 122(10),
801 549–558, doi:10.1061/(ASCE)0733-9429(1996)122:10(549), 1996.
- 802 Thomas, J. W., *Numerical Partial Differential Equations : Finite Difference Methods*,
803 Springer, New York, 1995.
- 804 Vanoni, V. A., *Sedimentation engineering*, Am. Soc. Coastal Eng., 1975.
- 805 Wilson, K., Analysis of bed-load motion at high shear stress, *Journal of Hydraulic Engi-*
806 *neering*, 113, 97103, 1987.

807 Wilson, K. C., Bed-load transport at high shear stress, in *Proc. A.S.C.E*, vol. HY6, ASCE,
808 1966.

809 Wilson, K. C., Mobile-bed friction at high shear stress, *Journal of Hydraulic Engineering*,
810 115(6), 825–830, doi:10.1061/(ASCE)0733-9429(1989)115:6(825), 1989.

811 Yalin, M. S., *Mechanics of sediment transport 2nd edition*, Pergamon Press, Ontario, 1977.

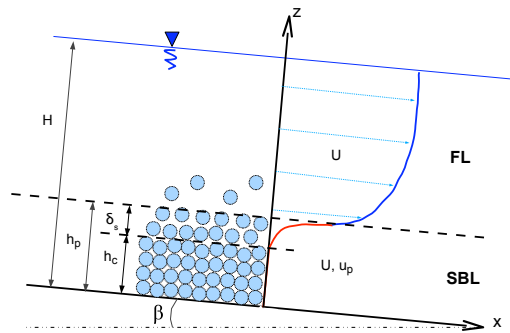


Figure 1. Sketch of unidirectional sheet flow

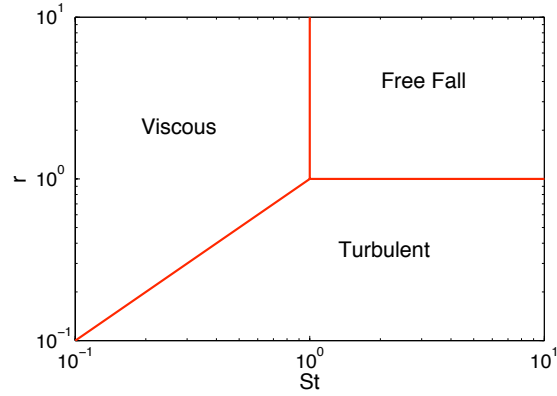


Figure 2. Phase diagram of the different flow regimes in the (St, r) plane for sheared immersed granular flows at imposed pressure [Andreotti et al., 2011].

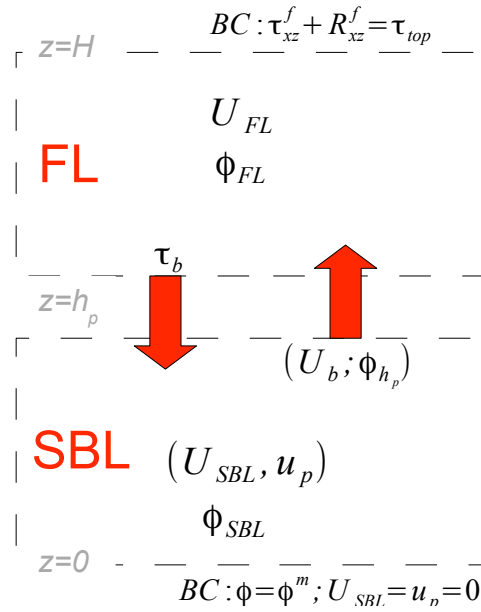


Figure 3. Sketch of the numerical resolution strategy.

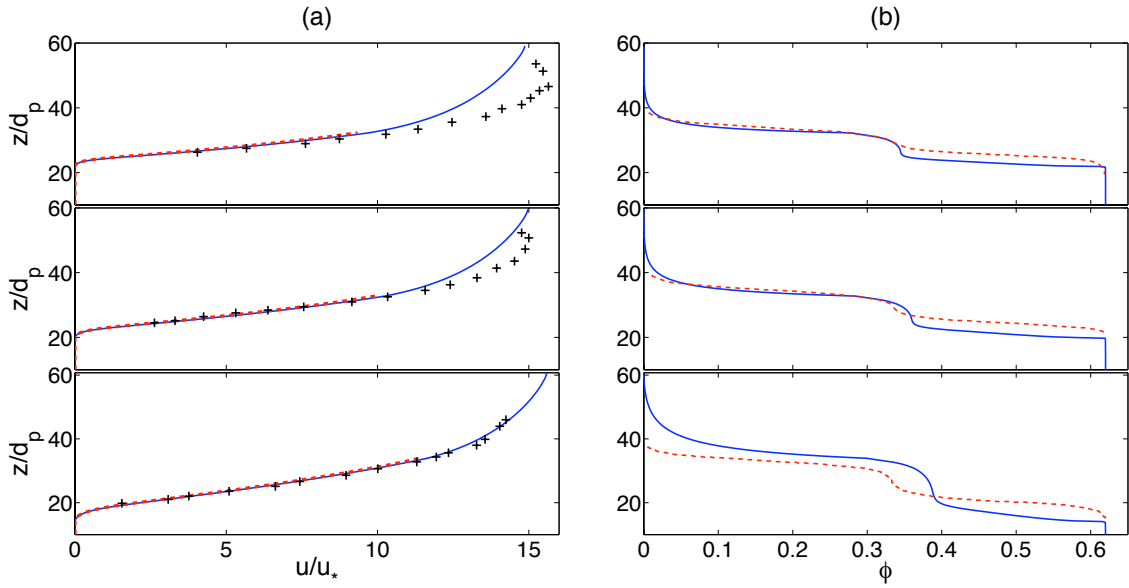


Figure 4. Comparison of the fluid (blue, —) and the particulate (red, - - -) velocity profiles between the present model and the measurements of *Sumer et al.* [1996] (+) in (a) and comparison of the concentration profiles predicted by the present model (blue, —) with *Hsu et al.* [2004]’s results (red, - - -) in (b). From top to bottom the left and right panels correspond to Run 82 ($\theta = 1.37$), Run 91 ($\theta = 1.65$) and Run 99 ($\theta = 2.3$) of *Sumer et al.* [1996]’s experiments.

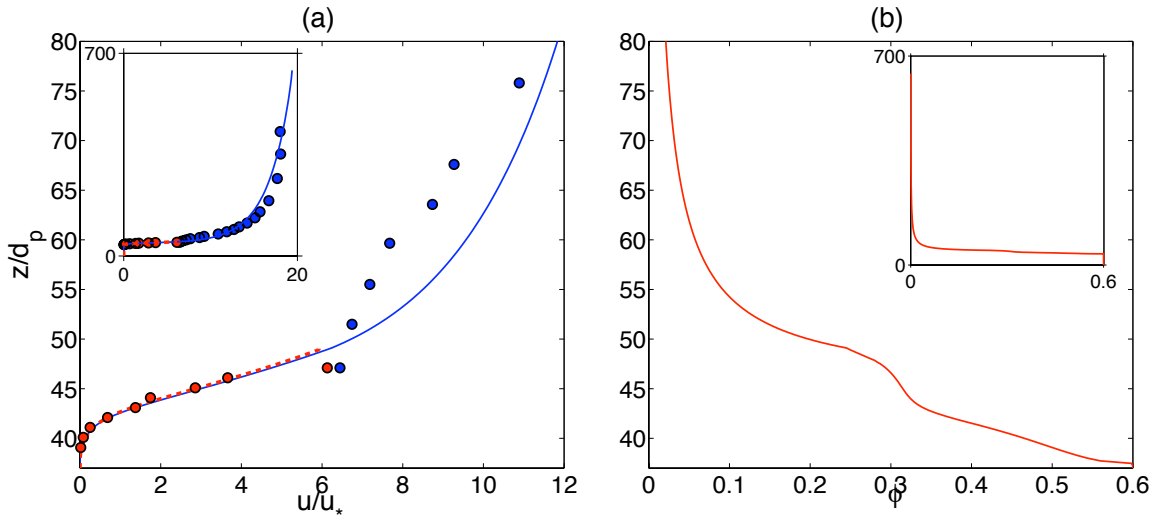


Figure 5. Comparison of the fluid (blue, —) and the particulate (red, - - -) velocity profiles between the present model and the measurements of *Cowen et al.* [2010] (red, ●) and (blue, ●) in (a) . The corresponding concentration profile is presented in (b).

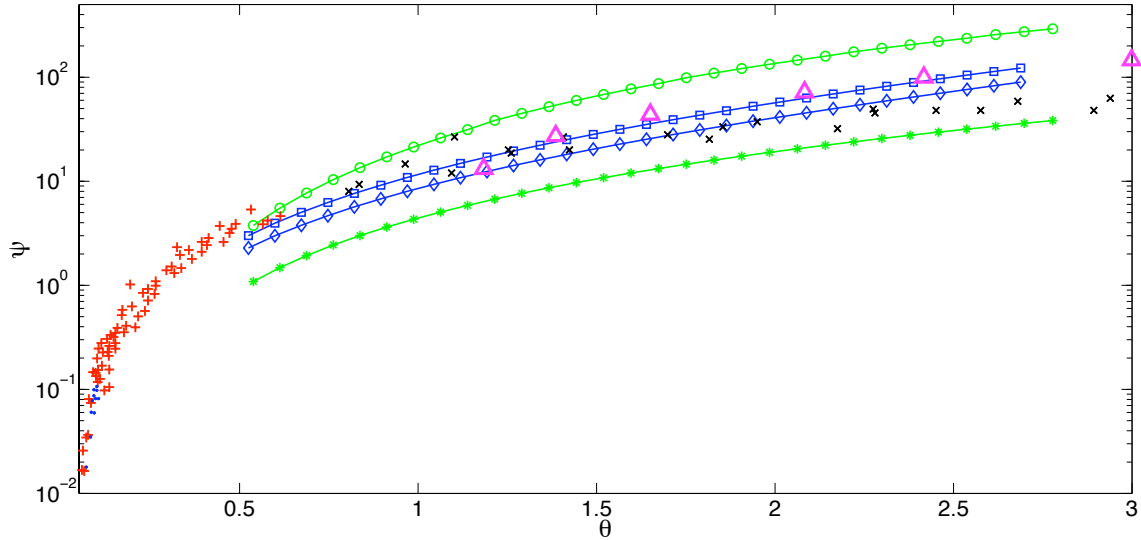


Figure 6. Dimensionless sediment transport rate $\psi = q_p/d_p\sqrt{(\rho_p - \rho_f)gd_p/\rho_f}$ and SBL contribution $\psi^{SBL} = q_p^{SBL}/d_p\sqrt{\rho_pgd_p/\rho_f}$ versus Shields parameter θ . Experimental data from *Meyer-Peter and Muller* [1948] (red, +), *Wilson* [1966] (x), *Gilbert* [1914] (blue, ●) synthesized in *Yalin* [1977]; model results from *Hsu et al.* [2004] (magenta, △); total load and bed-load results from the present model for sediment type A (blue, □; blue, ◇) and type B (green, ○; green, ★) respectively.

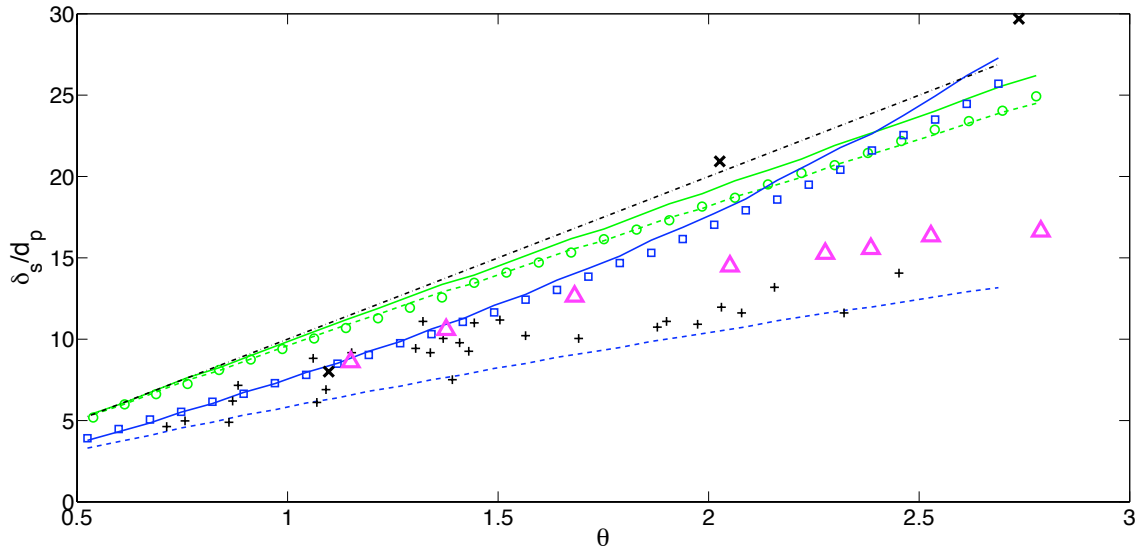


Figure 7. Comparison of the dimensionless sheet flow layer thickness $\delta_s/d_p = (h_p - h_c)/d_p$ between the present model results for sediment types A: numerical solution (blue, \square), equation (32) (blue, —), equation (33) (blue, - - -), and B: numerical solution (green, \circ), equation (32) (green, —), equation (33) (green, - - -), model results from *Hsu et al.* [2004] (magenta, \triangle), *Wilson* [1987]'s model predictions (- . -) and *Sumer et al.* [1996]'s data from visual observations (+) and from concentration profiles (x).

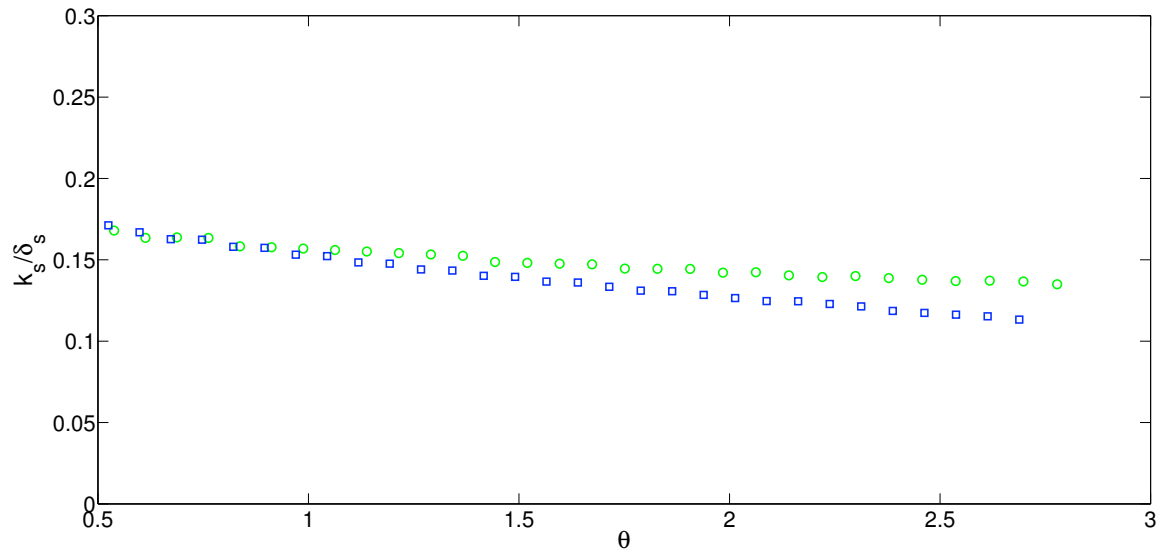


Figure 8. Dimensionless roughness k_s/δ_s versus Shields parameter θ for sediment types A (blue, \square) and B (green, \circ).

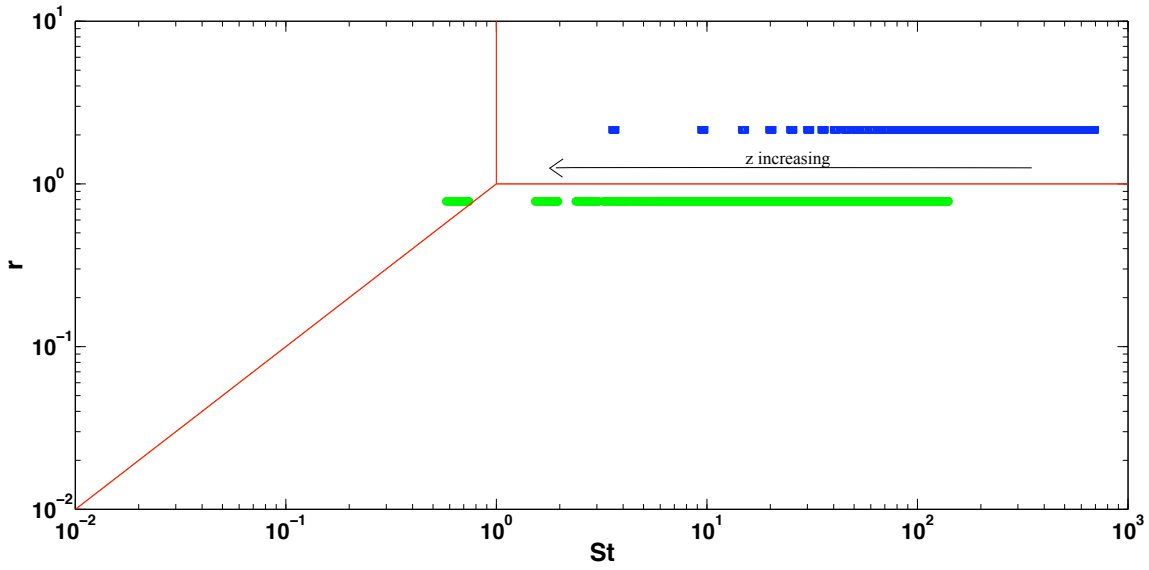


Figure 9. Phase diagram from *Andreotti et al.* [2011]. The limits in red (red, —) represent $St = 1, r = 1$ and $St = r$. Local regimes for sediment A (blue, \square) and B (green, \circ). The arrow shows the equivalent variation of vertical position .

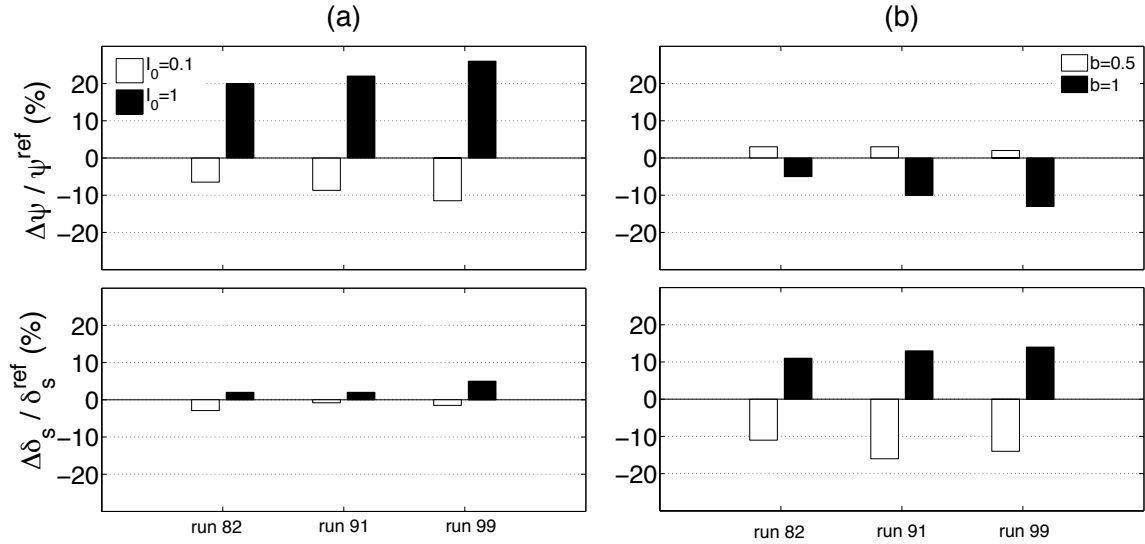


Figure 10. Sensitivity of the model results to the phenomenological parameters (a) I_0 and (b) b for the dimensionless sediment transport rate $\Delta\psi / \psi^{ref}$ and the thickness of the sheet flow layer $\Delta\delta_s / \delta_s^{ref}$. The values are relative to the reference simulation result (ψ^{ref} , δ_s^{ref}) obtained with $I_0 = 0.3$ and $b = 0.75$. The following values of the phenomenological parameters have been tested: $I_0 \in \{0.1; 1\}$ and $b \in \{0.5; 1\}$ for the three computed *Sumer et al.* [1996]'s runs.

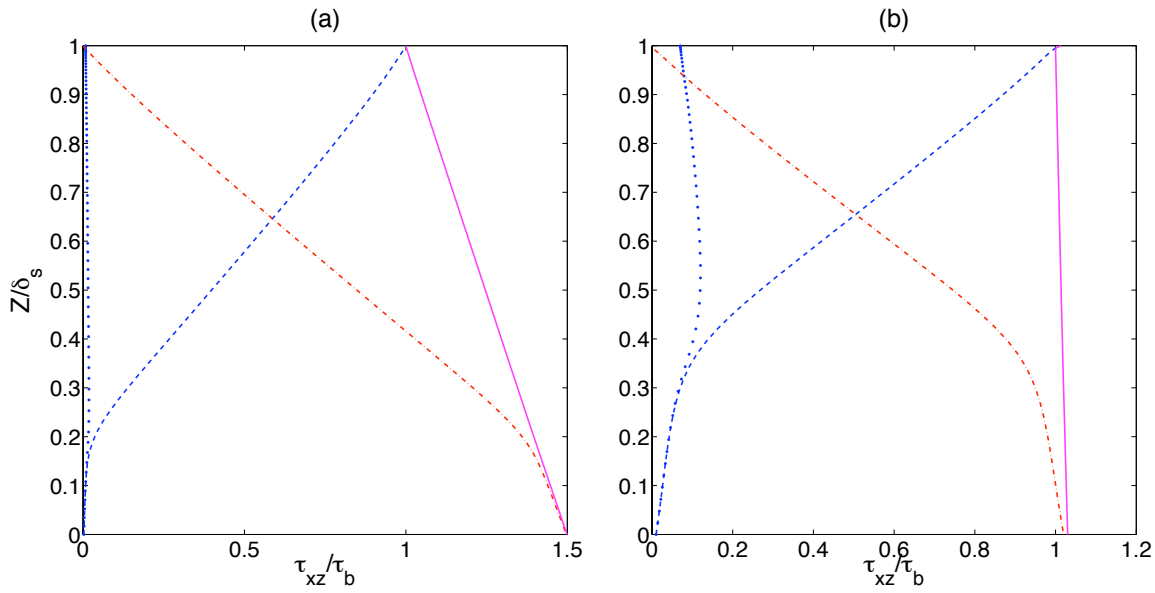


Figure 11. Results of the various contributions to the total mixture stresses inside the SBL, non-dimensionalized by the shear stress at the interface SBL/FL (τ_b), for run 91 of *Sumer et al.* [1996] (a) and *Cowen et al.* [2010]'s experiment (b). The vertical axis starts at the lower limit of the sheet and is non-dimensionalized by the thickness. (magenta, —) represents the mixture stresses, (red, - . -) represents the particulate stresses, (blue, - - -) represents the total fluid stresses and (blue, . . .) represents the viscous contribution to fluid stresses.

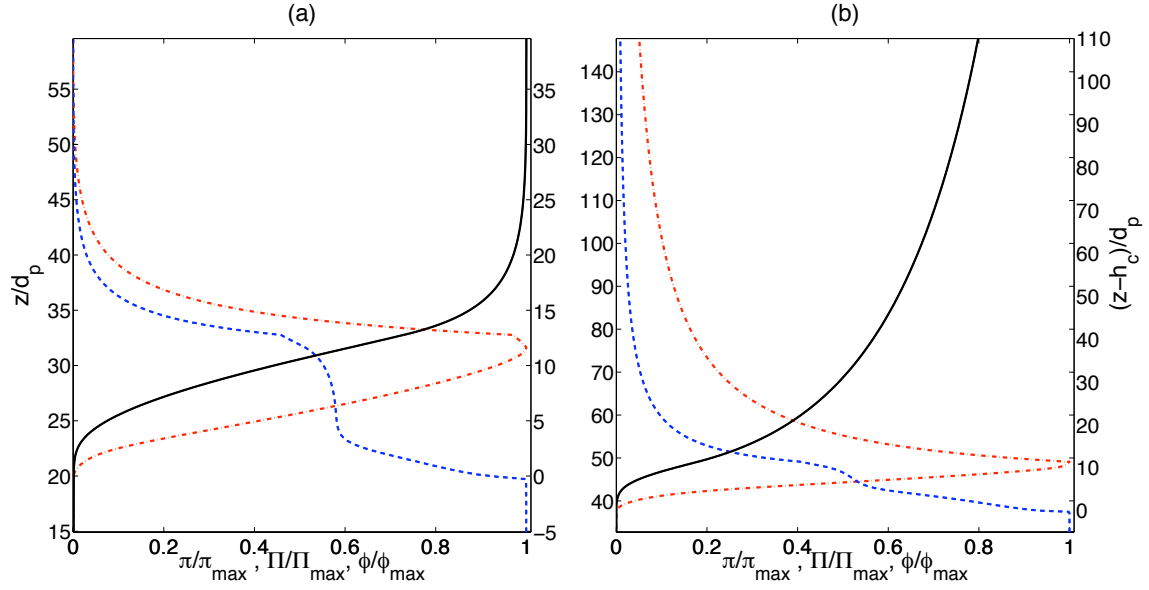


Figure 12. Concentration (blue, - -), sediment flux (red, - . -) and cumulated sediment flux (black, —) for *Sumer et al.* [1996]’s experiment, run 91 ($\theta = 1.64$) (a) and *Cowen et al.* [2010]’s experiment ($\theta = 1.25$) (b) with respectively $w_s/u_* = 0.94$ and $w_s/u_* = 0.44$

Table 1. Order of magnitudes for the estimates of the Stokes (St), r parameter and particulate Reynolds number (Re_p) in the sheet flow regime.

Param.	ρ_p/ρ_f	$\rho_p - \rho_f$	ϕ	d_p	δ_s
Unit	(-)	($kg.m^{-3}$)	(-)	(m)	(m)
O(●)	1	$10^2 - 10^3$	1	$10^{-4} - 10^{-3}$	$\sim 10 d_p$

Table 2. Sediment properties for *Sumer et al.* [1996] (type A) and *Cowen et al.* [2010]’s (type B) experiments.

Sediment type	Composition	Shape	d_p (mm)	ρ_p (kg/m^{-3})	ϕ_{max}	μ_s	w_s (m/s)
A	PMMA	Cylinders	2.6	1140	0.62	0.51	0.072
B	Glass	Beads	0.25	2600	0.6	0.3	0.0326

Table 3. Physical parameters for the simulations corresponding to *Sumer et al.* [1996] and *Cowen et al.* [2010]’s experiments.

Parameters (unit)	<i>Cowen et al.</i> [2010]	<i>Sumer et al.</i> [1996] run 82	<i>Sumer et al.</i> [1996] run 91	<i>Sumer et al.</i> [1996] run 99
Flow type	Free surface	Duct Flow	Duct Flow	Duct Flow
Sediment type	B	A	A	A
θ	1.25	1.37	1.64	2.30
u_* (m/s)	0.074	0.1	0.11	0.125
$\sin \beta$	0.0035	0.00715	0.0086	0.0119
H (cm)	12.5	17.4	17.5	17.6
h_p (cm)	1.2	8.4	8.5	8.8
ρ_f ($kg.m^{-3}$)	10^3	10^3	10^3	10^3
η_f ($kg.m^{-1}.s^{-1}$)	10^{-3}	10^{-3}	10^{-3}	10^{-3}

Table 4. Phenomenological and numerical parameters for the simulations corresponding to *Sumer et al.* [1996] and *Cowen et al.* [2010]’s experiments. The number in brackets refers to the equation containing the parameter.

	Sediment type	κ (18)	μ_2 (20)	I_0 (20)	b (24)	N_{FL}/N_{SBL}
<i>Sumer et al.</i> [1996]	A	0.35	0.7	0.3	0.75	143/150
<i>Cowen et al.</i> [2010]	B	0.41	0.64	0.3	0.75	197/150